Additive Manufacturing 38 (2021) 101842

Contents lists available at ScienceDirect

Additive Manufacturing

journal homepage: www.elsevier.com/locate/addma

Research Paper

Compression behavior and energy absorption of 3D printed continuous fiber reinforced composite honeycomb structures with shape memory effects

Chengjun Zeng [a], Liwu Liu [a], Wenfeng Bian [b,*], Jinsong Leng [c], Yanju Liu [a,*]

[a] Department of Astronautical Science and Mechanics, Harbin Institute of Technology (HIT), P.O. Box 301, No. 92 West Dazhi Street, Harbin 150001, People's Republic of China
[b] Department of Civil Engineering, Harbin Institute of Technology (HIT), Weihai 264209, People's Republic of China
[c] Center for Composite Materials and Structures, Harbin Institute of Technology (HIT), P.O. Box 3011, No. 2 YiKuang Street, Harbin 150080, People's Republic of China

ARTICLE INFO

Keywords:
3D printing
Continuous fiber
Honeycomb
Energy absorption
Shape memory

ABSTRACT

Three-dimensional (3D) printing is a potential rapid prototyping process that may replace traditional manufacturing processes to fabricate lightweight cellular structures with superior energy absorption performance. In the present work, continuous fiber reinforced composite honeycomb structures (CFRCHSs) with excellent shape memory properties were manufactured through a fused filament fabrication (FFF) technology, and their out-of-plane/in-plane compression behaviors and energy absorption characteristics were experimentally investigated. The results reveal that the failure process of the 3D printed CFRCHSs under in-plane loading is that the honeycomb cells collapse layer by layer along the loading direction , accompanied by the formation of a localized band. The crashworthiness analysis indicates that the 3D printed CFRCHSs outperform several competitive cellular topologies in the compression strength and specific energy absorption. A simplified analytical model for the in-plane compression strength of CFRCHSs was derived, and good agreement between measurements and predictions was observed. Additionally, the shape recovery tests demonstrate that the 3D printed CFRCHSs possess the potential as key elements of lightweight intelligent systems and adjustable energy absorbing devices.

1. Introduction

Lightweight cellular structures inspired by natural materials are increasingly used as the main load-bearing and protective members in the aerospace, marine engineering, and transportation industries due to their high specific stiffness/strength, excellent energy absorption capacity, and considerable thermal insulation [1–3]. The macroscopic performance of the cellular structures can be tailored by adjusting the microstructures and the raw materials of the cells. In general, these cellular structures are optimized to transform external work into internal energy of the structures through easier plastic deformation to avoid high stress caused by external loads, thereby achieving super energy absorption [4,5]. In the past few decades, a large number of cellular topologies have been available, such as honeycomb-like, truss, corrugated, chiral, hierarchical, or combined structures [6–10].

As an emerging rapid prototyping technology, additive manufacturing that also commonly referred to as three-dimensional (3D) printing allows the manufacture of cellular structures with spatially customized material characteristics and geometries [11]. The main attraction of 3D printing is that it provides unlimited geometric design freedoms and multi-scale molding capabilities, thus turning any geometric shape from the designer's imagination into reality. Many attentions and development activities are committed to the rapid manufacturing of metallic honeycomb and truss structures with considerable potential as lightweight energy absorbing products through 3D printing [12–15]. Extensive research has also been conducted to investigate the advantages of 3D printed polymer cellular structures [16,17].

Shape memory polymers (SMPs) are a class of active deformation materials with large deformation, variable stiffness, and shape memory effects, which can fix the temporary shape and recover their original shape under temperature control [18–20]. Recently, geometrically

* Corresponding authors.
E-mail addresses: bianwf@hit.edu.cn (W. Bian), yj_liu@hit.edu.cn (Y. Liu).

https://doi.org/10.1016/j.addma.2021.101842
Received 8 September 2020; Received in revised form 9 December 2020; Accepted 5 January 2021
Available online 8 January 2021

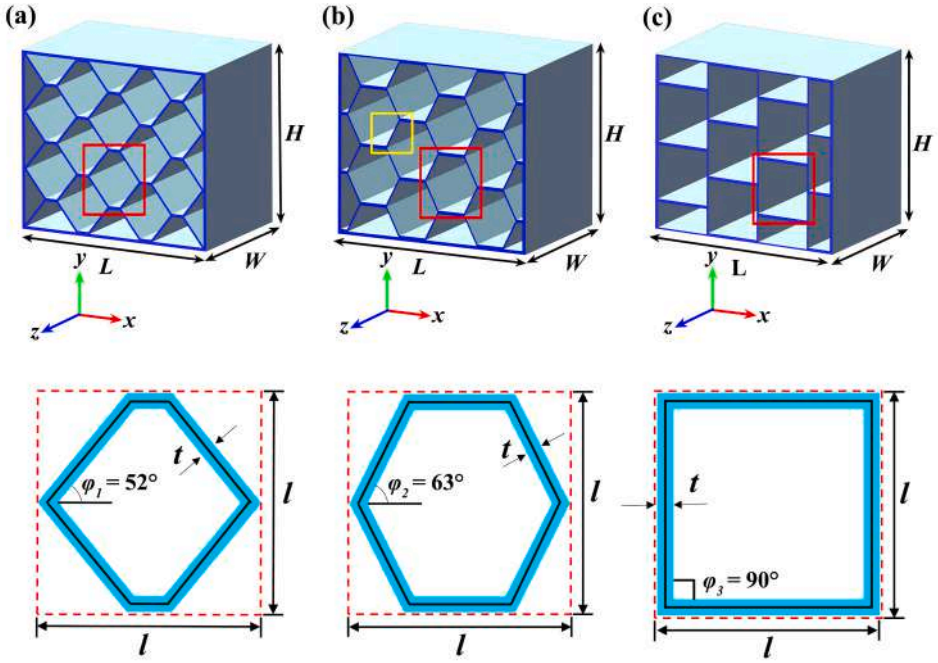

Fig. 1. The geometric configurations of the proposed honeycomb structures with various cells. (For interpretation of the references to colour in this figure legend, the reader is referred to the web version of this article.)

reconfigurable, functionally deployable, and mechanically tunable cellular metamaterials have been demonstrated by digital micro 3D printing with SMPs [21]. Incorporating materials with shape memory effects to the cellular structures could offer the structures the ability to modulate the mechanical properties in practical applications.

Compared with the traditional metals and soft materials used in 3D printing mentioned above, many newly developed composites such as continuous fiber reinforced composites possess higher specific mechanical properties and energy absorption capacities [22]. For this reason, the development of innovative 3D printing processes for continuous fiber reinforced composites and their lightweight structures has attracted many research activities [23–29]. The co-extrusion process based on fused filament fabrication (FFF) was developed to integrally manufacture continuous fiber reinforced thermoplastic composite (CFRTPC) honeycomb structures [25,27]. Another method for additive manufacturing of CFRTPC honeycomb structures is direct 3D printing based on FFF. In this process, the pre-impregnated thermoplastic fiber filaments are utilized to fabricate the honeycomb sandwich structures through fiber tension according to a customized path [29]. It is worth mentioning that recently a 3D printing technology called free-hanging has also been developed to manufacture CFRTPC lattice truss sandwich structures [30,31]. However, at present, extensive investigations on the compression failure behavior and energy absorption characteristics of the 3D printed continuous fiber reinforced composite honeycomb structures (CFRCHSs) are rarely presented. Moreover, there is no report about the 3D printed CFRCHSs with shape memory effects.

In the authors' previous work [32], an FFF-based 3D printing process was applied to prepare continuous carbon fiber reinforced shape memory polymer composites, and the electro-induced shape memory effect of the prepared composites was investigated. In the present study, we used this process to fabricate CFRCHSs with more sophisticated configurations, and comprehensively investigated their out-of-plane/in-plane compression properties and energy absorption characteristics. Since the matrix was a thermoplastic shape memory polymer, we preliminarily characterized the shape memory effects of the 3D printed CFRCHSs, which would promote their application in smart deformable structures and adjustable energy absorbing devices. Section 2 introduces the structural design, fabrication process, and experimental details of the 3D printed CFRCHSs. In Section 3, the out-of-plane/in-plane compression deformation modes and energy absorption properties of CFRCHSs are analyzed, and the shape memory effects of CFRCHSs are preliminarily evaluated. Finally, some guiding conclusions are drawn in Section 4.

Table 1
Geometrical parameters of the 3D printed CFRCHSs.

No.	l / mm	φ / °	L / mm	H / mm
1	18	52	65	57
2	18	63	65	57
3	18	90	65	57
4	24	52	85	75
5	24	63	85	75
6	24	90	85	75
7	30	52	105	93
8	30	63	105	93
9	30	90	105	93

2. Fabrication and experiment

2.1. Geometric description

Here, honeycomb structures with various cell configurations as shown in Fig. 1 are designed to investigate their compression properties and energy absorption capabilities. The honeycomb structure is defined by the dimensions in three main directions, namely length L, width W, and height H. There is the same number of cells in all honeycomb structures. The dimensions of the filled hexagonal cells are described by the element length l, the inclination angle φ, and the wall thickness t. Three different element lengths l (i.e., 18, 24, and 30 mm) and inclination angle φ (i.e., 52°, 63°, and 90°) are considered. It should be mentioned that the cell corresponding to $\varphi = 90°$ is rectangular, which is a limit case. Corresponding to three element lengths, three length L (i.e., 65, 85, and 105 mm) and height H (i.e., 57, 75, and 93 mm) are involved in this study. For instance, the length L and height H of the honeycomb

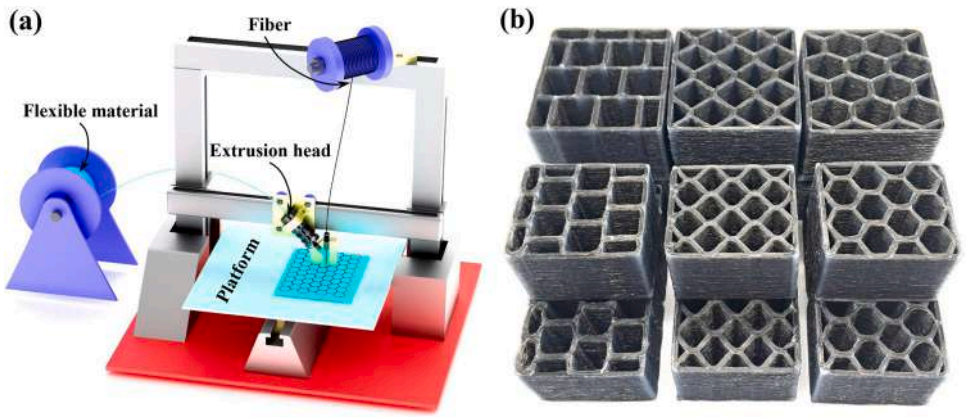

Fig. 2. Scheme of 3D printing for CFRCHSs. (a) 3D printing process for CFRCHSs. (b) Prepared CFRCHSs with various cell configurations.

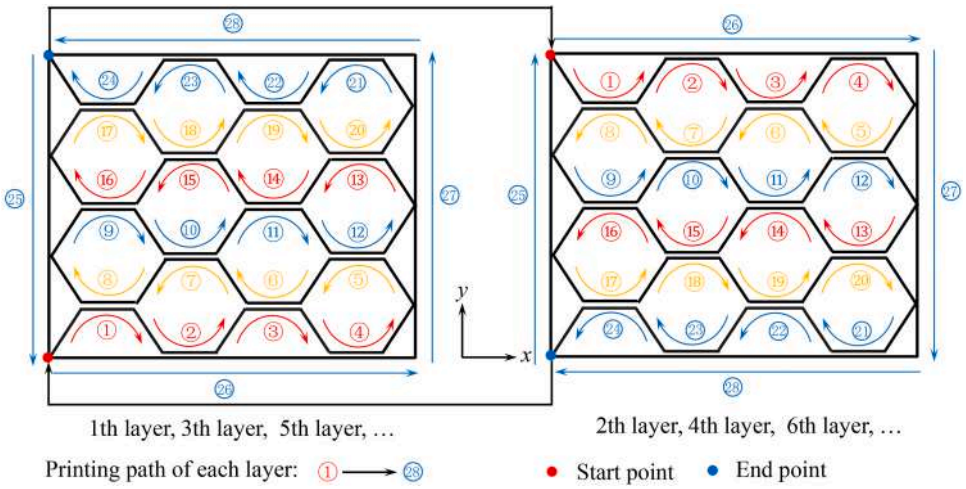

Fig. 3. Printing path design schemes for each layer of CFRCHSs.

structure are respectively 85 mm and 75 mm when the element length l = 24 mm. Besides, the width W of the honeycomb structures and the wall thickness t of the cells are selected to be 45 mm and 2.1 mm, respectively. Therefore, a total of nine sets of samples are set out in this study. The details of geometrical parameters are summarized in Table 1.

Relative density is an important indicator for evaluating lightweight cellular materials. The relative density $\overline{\rho}$ of the 3D printed CFRCHSs is calculated as follows:

$$\overline{\rho} = \frac{\rho_s}{\rho_m} = \overline{\rho}_c + 2(1-\overline{\rho}_c)\left(\frac{t}{L} + \frac{t}{H} - \frac{2t^2}{LH}\right) \tag{1}$$

where ρ_m is the density of the constituent material (3D printed carbon fiber reinforced polylactic acid (PLA) composite, $\rho_m = 1390\ \mathrm{kg/m^3}$), ρ_s denotes the absolute density of the 3D printed CFRCHSs, and $\overline{\rho}_c = \frac{2t(1+\sin\varphi-\cos\varphi)}{l(2\sin\varphi-\cos\varphi)}$ is the equivalent relative density of the honeycomb cell.

2.2. Fabrication methodology

In this work, an FFF-based 3D printer was used to integrally manufacture CFRCHSs. This printer is designed based on the co-extrusion process of continuous fiber and polymer, and there are two feeding channels connecting with the extrusion head, as shown in Fig. 2a. The flexible thermoplastic material and the continuous fiber bundle respectively enter the corresponding channels and converge in the liquefier. The thermoplastic material is melted by the heater and the extrusion force of the motor promotes the pre-impregnation of the fiber bundle and the molten resin. Then the printing task is completed by utilizing the fiber tension. Since the fiber cutting mechanism is not applied to the printer, it is necessary to predefine the printing path when manufacturing a complicated honeycomb structure. The printing paths for the odd and even layers are different because the printing is completed without nozzle jumping. These two path schemes are shown in Fig. 3. The printing of single layer is completed in the x-y plane, and the printing path begins from the "start point" and ends at the "end point" according to the sequence number. After the single-layer printing is finished, the nozzle moves 0.4 mm in the z direction, and prints continuously with the "end point" of the old layer as the "start point" of the new layer. The construction of three-dimensional objects is realized through a layer-by-layer stacking mechanism. CFRCHSs were fabricated by stacking a total of 113 layers. In the 3D printing process, the process parameters were determined as: a printing speed of 100 mm/min, a nozzle temperature of 210 °C, thereby obtaining weighted printing accuracy and efficiency [27].

Continuous carbon fibers hold outstanding axial mechanical properties and thermal stability. So in this study, T300B–3000–40B carbon fiber bundles manufactured by Toray Japan Co., Ltd. were used as the reinforcing material for the 3D printed honeycomb structures. The applied thermoplastic material was semi-crystalline PLA filament prepared by Harbin Institute of Technology, which possessed excellent variable stiffness capability and shape memory effects [19]. Differential scanning calorimetry (DSC) and thermal gravimetric analysis (TGA) measurements were performed to systematically characterize the thermal properties of PLA filament, from which it could be found that the

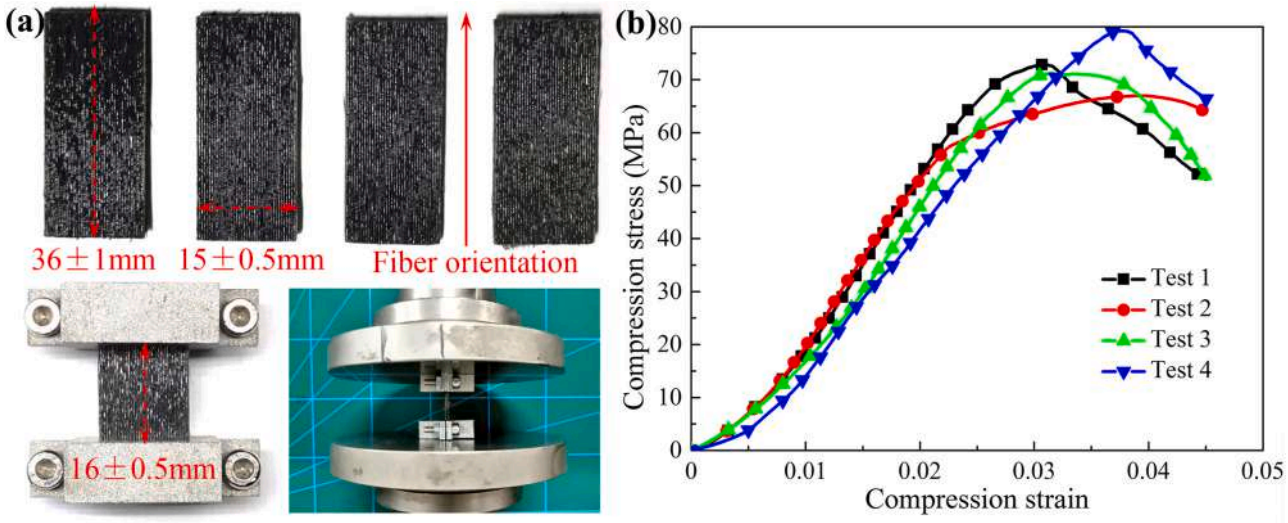

Fig. 4. Axial compression test of the parent material. (a) Samples and experimental apparatus. (b) Measured compression stress-strain curves.

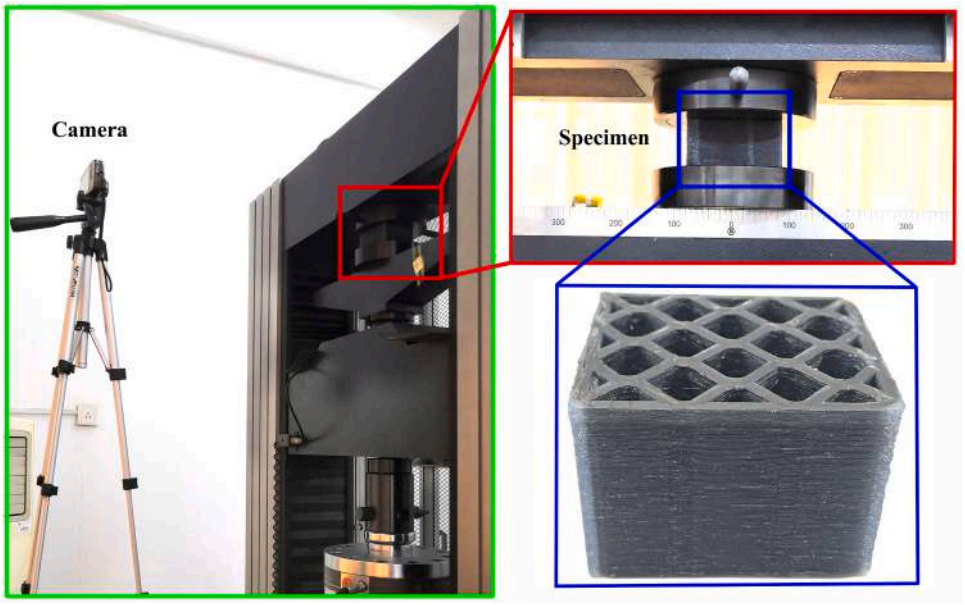

Fig. 5. Quasi-static out-of-plane compression test setup for the 3D printed CFRCHSs specimen.

glass transition temperature (Tg), crystallization temperature, melting temperature, and degradation temperature of the filament were about 63 °C, 110 °C, 170 °C, and 345 °C, respectively [19]. Fig. 2b presents CFRCHSs with various geometric configurations prepared by the proposed 3D printing method.

2.3. Experimental measurements

2.3.1. Parent material properties

The compression performance of the 3D printed CFRCHSs is not only related to the geometric configuration of the cell, but also depends on the mechanical properties of the parent material. Therefore, the compression tests of the 3D printed continuous carbon fiber reinforced composite samples were performed to determine the compression modulus and strength of the parent material. The fabrication process of the rectangular samples is similar to that of the honeycomb wall, and the fiber infill orientation is consistent with the loading direction, as shown in Fig. 4a. The geometric size of the samples is 36 × 15 × 2.1 mm, and the fiber volume fraction is about 13%. In order to keep the rectangular sample vertical during compression, the clamping apparatus similar to [33] was used to fix both ends of the sample. Four samples were tested, and the compression stress-strain curves obtained are presented in Fig. 4b. The measured mean compression modulus E_s of the parent material is 3.07 GPa with a standard deviation of 0.25 GPa, and the mean compression strength σ_c is 72.1 MPa with a standard deviation of 4.4 MPa.

2.3.2. Out-of-plane compression tests

3D printed CFRCHSs with different geometries and cell configurations were subjected to the quasi-static out-of-plane compression tests to investigate their crushing modes and generate corresponding load-displacement curves, from which related crashworthiness parameters such as energy absorption (*EA*), specific energy absorption (*SEA*), and crushing force efficiency (*CFE*) were obtained. The out-of-plane compression tests were performed on a CMT 5305 electronic universal testing machine with a load cell of 300 kN according to ASTM D1621 standard. Fig. 5 exhibits the compression test setup and the 3D printed CFRCHSs specimen placed between the platens, where the specimen is

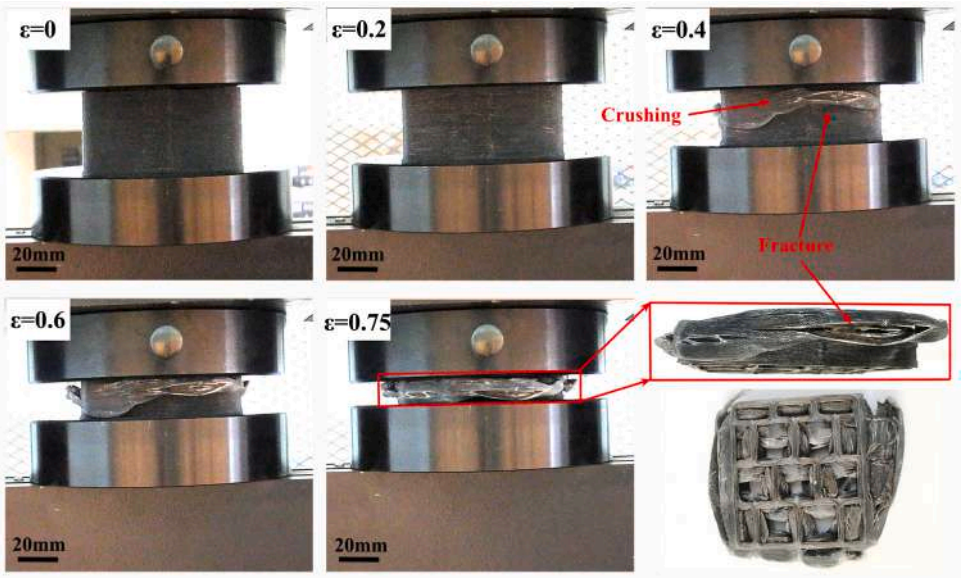

Fig. 6. The typical out-of-plane progressive compression deformation of the 3D printed CFRCHSs.

compressed by applying a uniform pressure at a displacement rate of 4 mm/min. All specimens were compressed up to 75% of their original widths. Also, a digital camera was used to record the deformation modes of all samples during out-of-plane compression. The indices for evaluating the compression performance of the 3D printed CFRCHSs are available from the experimentally measured force-displacement curves. According to the area under the force-displacement curve, *EA* is calculated as follows

$$EA = \int_0^{\delta_d} F d\delta \tag{2}$$

where δ_d represents the maximum compression displacement at the onset of the densification stage and F denotes the compression load. *SEA* is the ratio of *EA* to the mass m of the sample, as shown below

$$SEA = \frac{EA}{m} \tag{3}$$

The mean crushing force (*MCF*) is defined as

$$MCF = \frac{1}{\delta_d}\int_0^{\delta_d} F d\delta \tag{4}$$

CFE is defined as the ratio of *MCF* to initial peak force (*IPF*) as

$$CFE = \frac{MCF}{IPF} \tag{5}$$

2.3.3. In-plane compression tests

When the honeycomb structure is used as an energy absorbing device in engineering, crushing may occur in any direction of the structure. It is also essential to understand the impact of the cell configuration on the in-plane compression behavior of the honeycomb structure beyond its out-of-plane behavior. Hence, quasi-static in-plane compression tests were performed to investigate the in-plane crushing behavior and energy absorption characteristics of the 3D printed CFRCHSs. The experimental procedure is similar to that of the out-of-plane compression tests. But it is worth noting that the samples with three different heights H (i.e., 57, 75, and 93 mm) have maximum compression displacements of 42.8, 56.3, and 69.8 mm, respectively. The local morphology of the samples after compression failure was characterized by VEGA3 TESCAN scanning electron microscopy (SEM).

2.3.4. Shape recovery tests

The 3D printed CFRCHSs with only several honeycomb cells were shaped by an electronic testing machine (ZWICK-010) equipped with an environmental chamber at a constant temperature of 70 °C. The original length L_{ori} and height H_{ori} of the samples are 68 mm and 48 mm, respectively, and the honeycomb parameters are $l = 24$ mm and $\varphi = 52°$. In addition, the out-of-plane width W_{ori} of the sample is 16 mm, and the wall thickness t of the cell is 2.1 mm. The loading mode was in-plane compression with a rate of 2 mm/min, and the amount of compression was 50% of the original height of the samples. After loading, the samples were kept in a deformed shape by reducing the temperature to room temperature. The shape recovery tests were conducted in a 70 °C water bath, and the deployment process of the samples was recorded by a camera.

3. Results and discussion

3.1. Out-of-plane compression properties

3.1.1. Deformation modes

Experimental results indicate that the 3D printed CFRCHSs with different cell configurations exhibit similar deformation patterns when subjected to out-of-plane compression. It can be observed from Fig. 6 that the out-of-plane deformation mode of CFRCHSs is a combination of lateral shearing failure and progressive folding failure. The layer-by-layer 3D printing process resulted in weak lateral mechanical properties of CFRCHSs, so transverse plastic cracking occurred on the outer surface of the samples. Nonetheless, there are a few significant advantages. For example, there is almost no fracture at the connection points between adjacent cells inside the 3D printed CFRCHSs during the crushing process due to the excellent bonding performance between the various regions of the honeycomb structure imparted by the integrated manufacturing process.

The force-displacement and equivalent stress-strain responses of the 3D printed CFRCHSs with various design variables tested in the out-of-plane compression experiments are plotted in Figs. 7 and 8, respectively. Equivalent out-of-plane compression stress is defined as $\sigma_{out} = F/A$, where F is the compression load and A is the equivalent cross-sectional area which can be calculated by $A = L \times H$. In general, all force-displacement curves and stress-strain curves possess similar evolutionary patterns, which can be divided into three different stages: initial elastic deformation, deformation plateau, and densification. Before

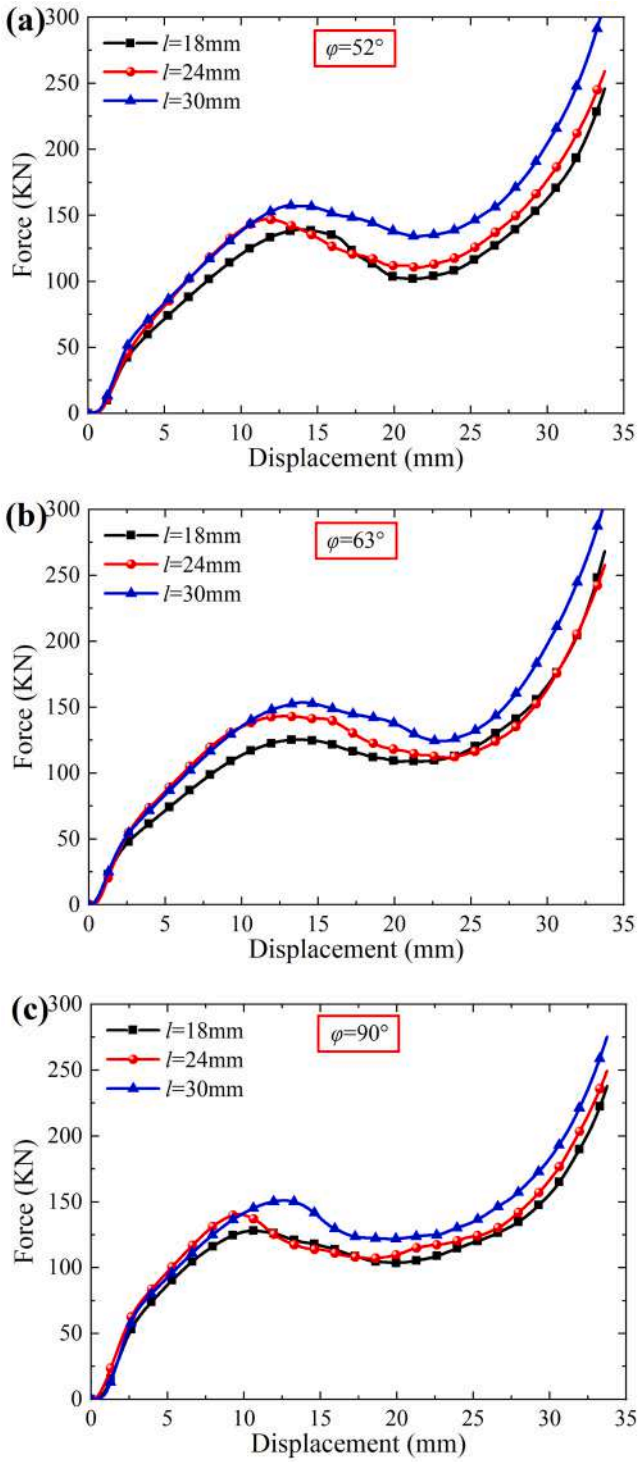

Fig. 7. Typical force-displacement curves of the 3D printed CFRCHSs with various inclination angles under out-of-plane compression. (a) $\varphi = 52°$. (b) $\varphi = 63°$. (c) $\varphi = 90°$.

getting to the initial peak force, the crushing force increases rapidly during the elastic deformation stage. Once the initial peak force is reached, the crushing force decreases due to the progressive failure of the structure, which is followed by a stable deformation process with strain-softening.

It can be observed from Fig. 8a–c that the element length of the 3D printed CFRCHSs exerts a conspicuous effect on the evolution of the deformation plateau. That is, the greater the element length is, the longer and smoother the deformation plateau is. In fact, the larger the element length is, the smaller the relative density of CFRCHSs is. The small relative density leads to the delay of densification, which in turn preserves a longer deformation plateau. Besides, the inclination angle of the cells also affects the evolution of the deformation plateau. By comparing the stress-strain curves for samples with the same element length and different inclination angles shown in Fig. 8d–f, it can be found that the sample with an inclination angle of 52° has a shorter deformation plateau, which means poor compression resistance. This phenomenon is probably attributed to the weak adhesive performance caused by the small contact area among the cells of the structure with an inclination angle of 52°.

3.1.2. Energy absorption

One of the potential applications of the 3D printed CFRCHSs is an energy absorbing device. When designing a lightweight structure, choosing appropriate cellular parameters contributes to a competitive specific energy absorption capacity. Fig. 8 shows that the equivalent compression strain is about 60% at the onset of the densification stage, so the crashworthiness parameters are calculated with $\delta_d = 27$ mm. Fig. 9 depicts the measured crashworthiness parameters of the 3D printed CFRCHSs with various honeycomb geometries under out-of-plane loading. It can be seen from Fig. 9a that the inclination angle slightly affects *IPF* when the element lengths of CFRCHSs are the same. For instance, when the element length l is set to 24 mm, *IPF* of CFRCHSs with different inclination angles ($\varphi = 52°$, 63°, and 90°) is 147.0 kN, 143.0 kN, and 140.4 kN, respectively. The element length exerts a significant impact on *IPF*. The larger element length means greater geometric size and mass of the structures, so *IPF* increases with the increase of the element length. Similar trends in *EA* are observed in Fig. 9b. When the inclination angle is fixed, the larger element length corresponds to the significantly improved energy absorption. For example, when the inclination angle is 63°, *EA* of CFRCHSs with the element lengths of 24 mm and 30 mm increases by 10.9% and 18.6%, respectively, compared with that of CFRCHSs with an element length of 18 mm.

SEA is a decisive parameter for evaluating the crashworthiness of a lightweight structure, which represents the energy absorption capacity of the structure per unit mass. From Fig. 9c, it can be found that an increase in the element length will lead to an obvious degradation in the out-of-plane *SEA* of the 3D printed CFRCHSs. It is desirable to appropriately reduce the feature size of the honeycomb cell to achieve greater specific energy absorption capacity. *CFE* is another major crashworthiness parameter, which describes the uniformity of the crushing force during loading. A higher *CFE* value may reduce undesired scattered acceleration and potential damage to the structure. The experimental results in Fig. 9d indicate that when the element length is set to 30 mm, the inclination angle affects *CFE* of the 3D printed CFRCHSs little. When the element length is 18 mm or 24 mm, the honeycomb structure with an inclination angle of 52° possesses a lower *CFE* than that with an inclination angle of 63° or 90°.

3.1.3. Comparison with competing topologies

It is instructive to compare the compression performance of the 3D printed CFRCHSs in the present work with the competitive cellular topologies prepared by different processes. Fig. 10 compares the out-of-plane compression strength and out-of-plane *SEA* of the 3D printed CFRCHSs with other competitive cellular topologies including carbon fiber reinforced polymer (CFRP) hierarchical honeycomb [6], 3D printed PLA honeycomb [9], Aluminum (Al) foam filled CFRP tube [34], Al honeycomb filled CFRP tube [34], stiffened syntactic foam [35], metallic square-honeycomb [36], CFRP hexagon honeycomb [1], hierarchical thermoplastic honeycomb [37], Al hexagon honeycomb [38], and Al hierarchical honeycomb [39].

Note that the 3D printed CFRCHSs significantly outperform the pure PLA honeycomb structures fabricated by 3D printing in terms of out-of-plane compression strength and SEA, which indicates that the 3D

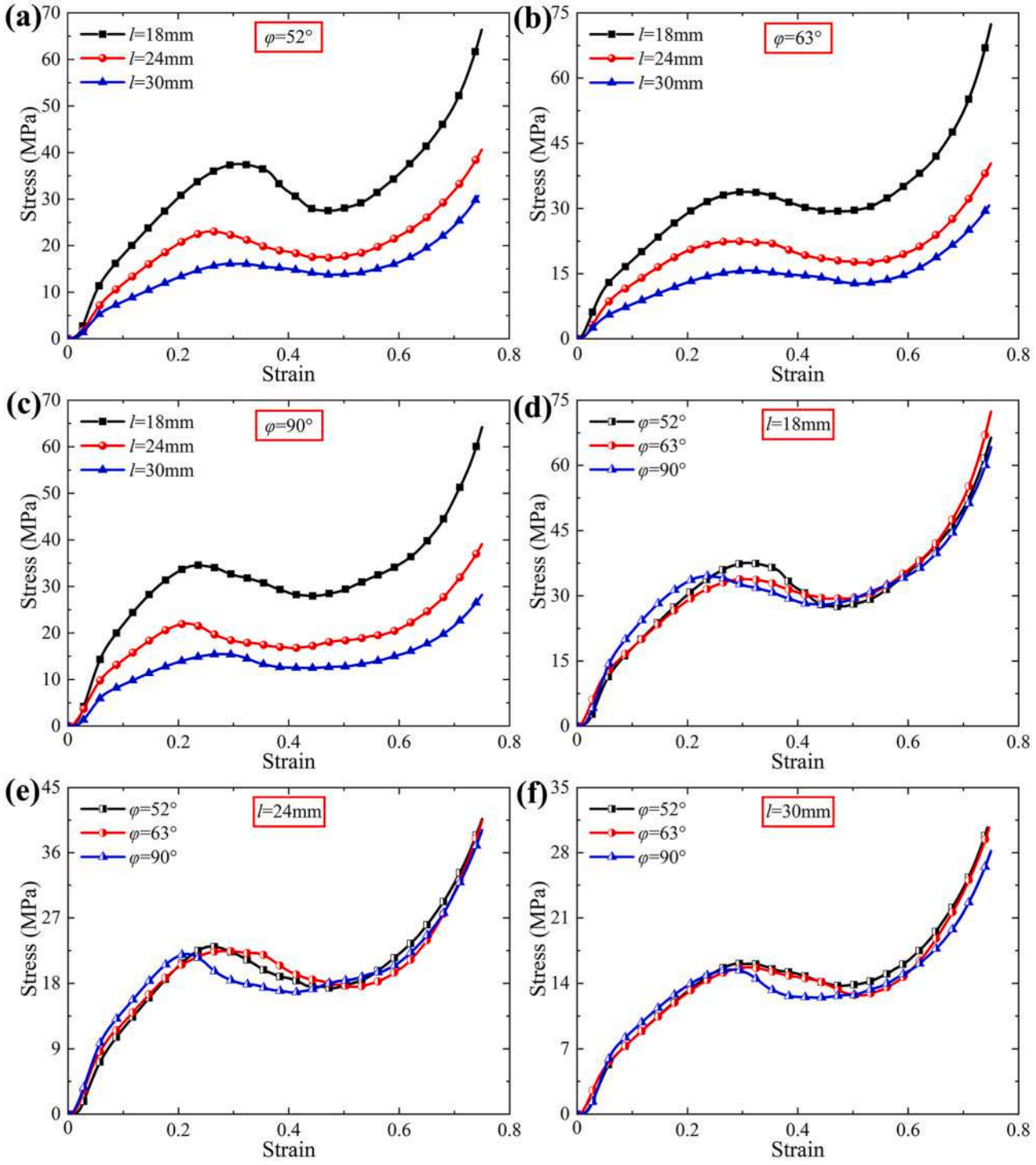

Fig. 8. The equivalent stress-strain responses of the 3D printed CFRCHSs under out-of-plane compression.

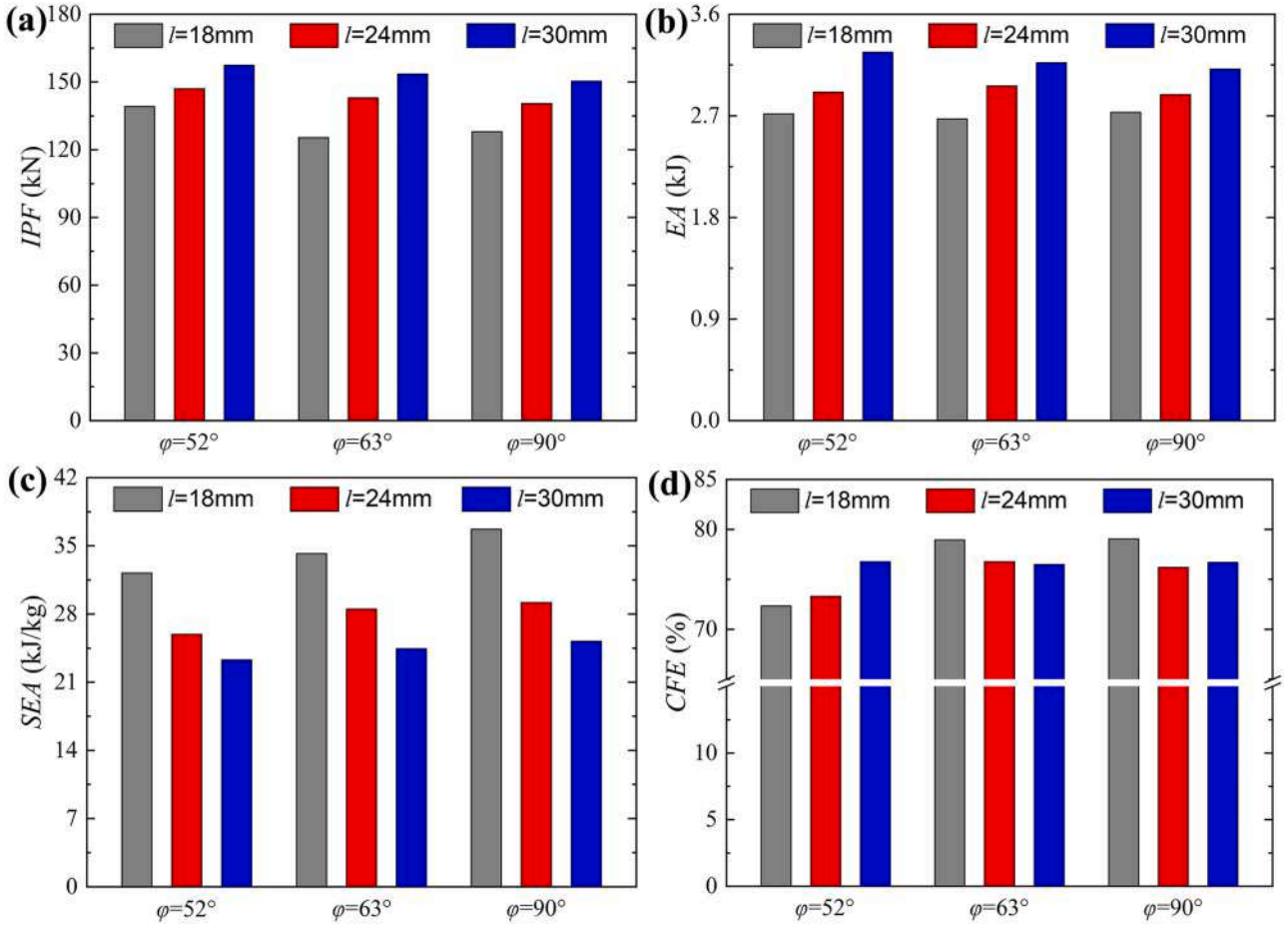

Fig. 9. Comparison of the crashworthiness parameters of the 3D printed CFRCHSs under out-of-plane compression. (a) Initial peak force *IPF*. (b) Total energy absorption *EA*. (c) Specific energy absorption *SEA*. (d) Crushing force efficiency *CFE*.

printing process for continuous fiber reinforced composites has broad prospects in the rapid manufacturing of the lightweight structures with high strength and high energy absorption. Obviously, it must be admitted that the density of the 3D printed CFRCHSs is relatively high compared to CFRP honeycomb, thermoplastic honeycomb, and aluminum honeycomb structures manufactured by traditional processes. Nevertheless, the outstanding out-of-plane compression strength and specific energy absorption capacity can still make them potential candidates for energy absorption applications.

3.2. In-plane compression properties

3.2.1. Deformation modes

The in-plane compression stress-strain curves of the 3D printed CFRCHSs with different element lengths are plotted in Fig. 11. Equivalent in-plane compression stress is defined as $\sigma_{in} = F/S$, where S is the equivalent cross-sectional area which can be calculated by $S = L \times W$. The evolution of the curves can also be divided into three distinct stages. Compared with the out-of-plane compression cases, there is no obvious plateau evolution in the in-plane compression stress-strain curves, which is mainly caused by the complicated failure modes of the honeycomb cells. It can be seen from Fig. 11 that the sample with element length $l = 18$ mm has higher initial peak stress than the sample with $l = 24$ mm and enters the densification stage earlier.

A series of deformed configurations of the 3D printed CFRCHSs concerning the moments when the square and circle symbols in Fig. 11 are located are presented in Fig. 12. It is observed that samples with different element lengths and the same inclination angle show high similarity in the in-plane compression deformation modes. When the initial peak stress is reached, the buckling and matrix failure of the honeycomb walls begin to occur (mode I). With further compression, the honeycomb walls break and partially collapse, which is accompanied by the formation of a lateralized localized band (mode II). Note that the stress precipitously decreases to a local minimum during this process. Subsequently, stress undulations occur, which demonstrates the further expansion of the localized band and the densification of the honeycombs. Eventually, all crushed honeycomb walls come into contact with each other and the structure enters the densification stage, so the stress required for further compression rises rapidly. Fig. 13 shows the local micromorphology of the 3D printed CFRCHSs after in-plane compression testing, from which it can be observed that the plastic hinges and matrix fracture generated at the nodes cause the collapse of CFRCHSs.

The in-plane compression responses of the 3D printed CFRCHSs with various honeycomb inclination angles are presented in Fig. 14. It can be observed that the structure with an inclination angle of 90° holds higher initial peak stress and a more severe post-peak failure evolutionary process than the structure with an inclination angle of 52°. This phenomenon can be attributed to the fact that the honeycomb wall corresponding to an inclination angle of 90° under in-plane loading is only subjected to axial load without lateral shearing. Fig. 15a shows the

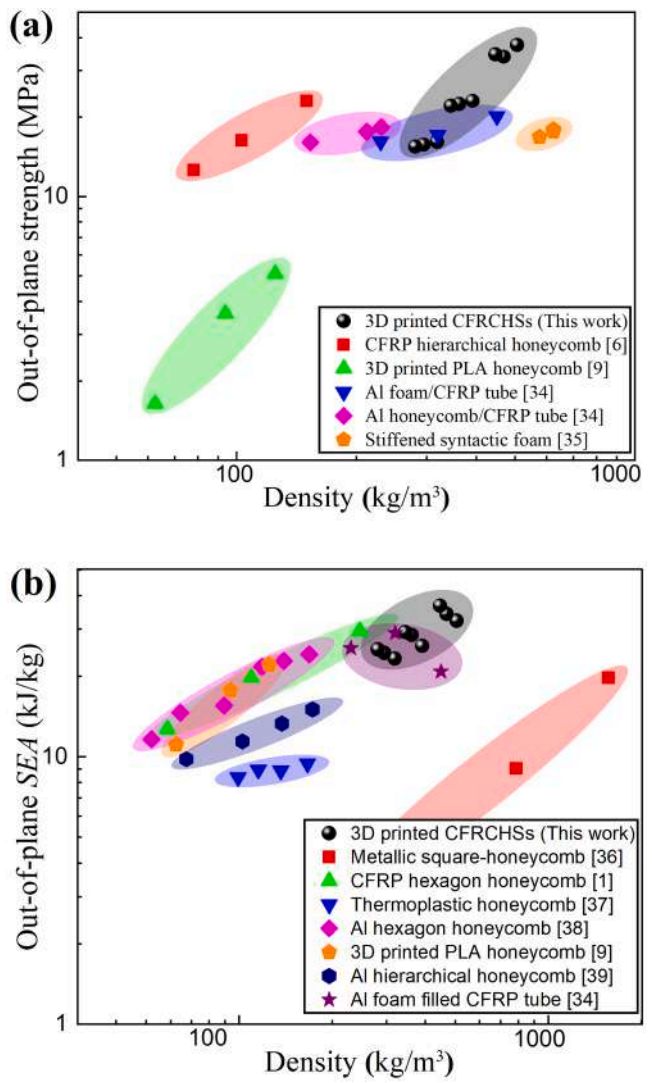

Fig. 10. Comparison of the out-of-plane compression properties between the 3D printed CFRCHSs and the competitive cellular topologies. (a) Compression strength. (b) Specific energy absorption *SEA*.

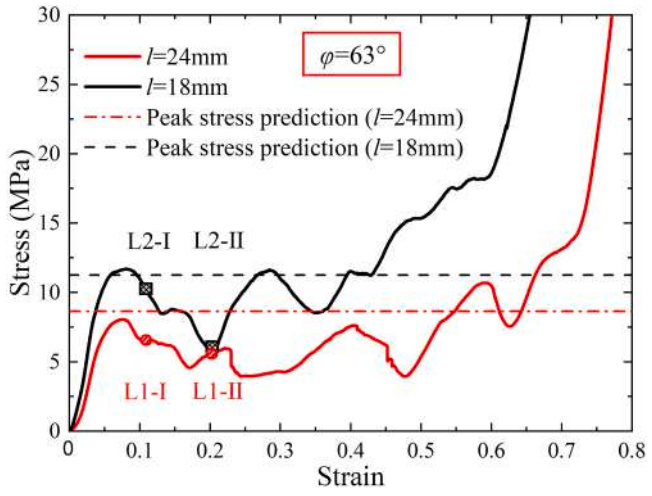

Fig. 11. The equivalent stress-strain curves of the 3D printed CFRCHSs with various element lengths under in-plane compression.

failure process of the structure with an inclination angle of 52° under in-plane compression. The overall collapse of the structure and the formation of the lateralized localized band are caused by the shear fracture of the honeycomb webs at the nodes.

Different from the failure mode of the structure with $\varphi = 52°$, Fig. 15b indicates that the in-plane compression failure of the structure with $\varphi = 90°$ is mainly caused by the fracture of the vertical webs in the middle. From Fig. 15b, it can be observed that the fibers are pulled out at the break of the honeycomb webs, which demonstrates that the interface bonding between the continuous carbon fibers and the molten PLA is imperfect during the 3D printing process. Therefore, the manufacturing process needs to be further developed to improve the bonding strength of the 3D printed composite members at the fiber/matrix interface.

3.2.2. Energy absorption

Corresponding to the honeycomb structures with three different element lengths (i.e., $l = 18$, 24 and 30 mm), the δ_d was respectively set to 34.2, 45.0 and 55.8 mm when calculating the in-plane energy absorption. Fig. 16 lists the *EA* and *SEA* of the 3D printed CFRCHSs with various element lengths and inclination angles under in-plane compression, which are considered to be crucial for crashworthiness design. Overall, it is found that the structural parameters of the honeycomb cells have similar effects on *EA* and *SEA* during in-plane compression. When the element lengths are the same, the honeycomb structure with $\varphi = 63°$ exhibits a significantly high energy absorption capacity. By comparing the energy absorption characteristics of the structures with the same honeycomb inclination angle and different element lengths, it is found that the element length can vary *EA* insignificantly but *SEA* drastically. That is, as the element length increases, *EA* of the 3D printed CFRCHSs is slightly lower, but *SEA* is greatly reduced. Therefore, setting the structural parameters to $l = 24$ mm and $\varphi = 63°$ is a feasible solution for lightweight and high energy absorption applications.

3.2.3. Comparison with competing topologies

Fig. 17 compares the in-plane compression strength and in-plane *SEA* of the 3D printed CFRCHSs with these of other commercial cellular configurations [15,40–48]. From Fig. 17a, it can be observed that the 3D printed CFRCHSs are superior to 3D printed polymeric honeycomb [40], 304 stainless steel (SS) corrugation [41], CFRP pyramidal core [42], 304 SS hourglass truss [43], CFRP Y-shaped core [44], and body-centered cubic with vertical strut (BCCZ) panel fabricated by selective laser melting (SLM) [15] in terms of the in-plane compression strength, and even comparable to 3D printed steel lattice [45]. Moreover, the 3D printed CFRCHSs possess a lower density than 3D printed steel lattice, showing a great application potential. Besides, the comparison of the in-plane *SEA* presented in Fig. 17b proves that the 3D printed CFRCHSs prominently outperform the 304 SS corrugation [41], Al corrugated sandwich panel [46], 3D printed polymeric honeycomb [47], Miura-ori based metamaterial [48], and 3D printed steel lattice [45].

3.2.4. Prediction of the compression strength

The analytical expression of the equivalent compression modulus of CFRCHSs is given by first analyzing the elastic deformation of a single honeycomb web, and then expanding the results to evaluate the overall effective characteristics. Fig. 18a and b are schematic diagrams of a quarter honeycomb cell and the inclined web of the cell under in-plane compression loading, respectively, which are taken from the area marked with a yellow rectangle in Fig. 1b. The thickness of the cell web is t, the length of the inclined part is λ and the lateral width is b. The symmetry condition indicates that the right end of the support can only move freely in the z-direction. Applying a virtual displacement δ in the z-direction, the axial force F_N of the support member is

$$F_N = \frac{E_s bt}{\lambda}\delta \sin\varphi \tag{6}$$

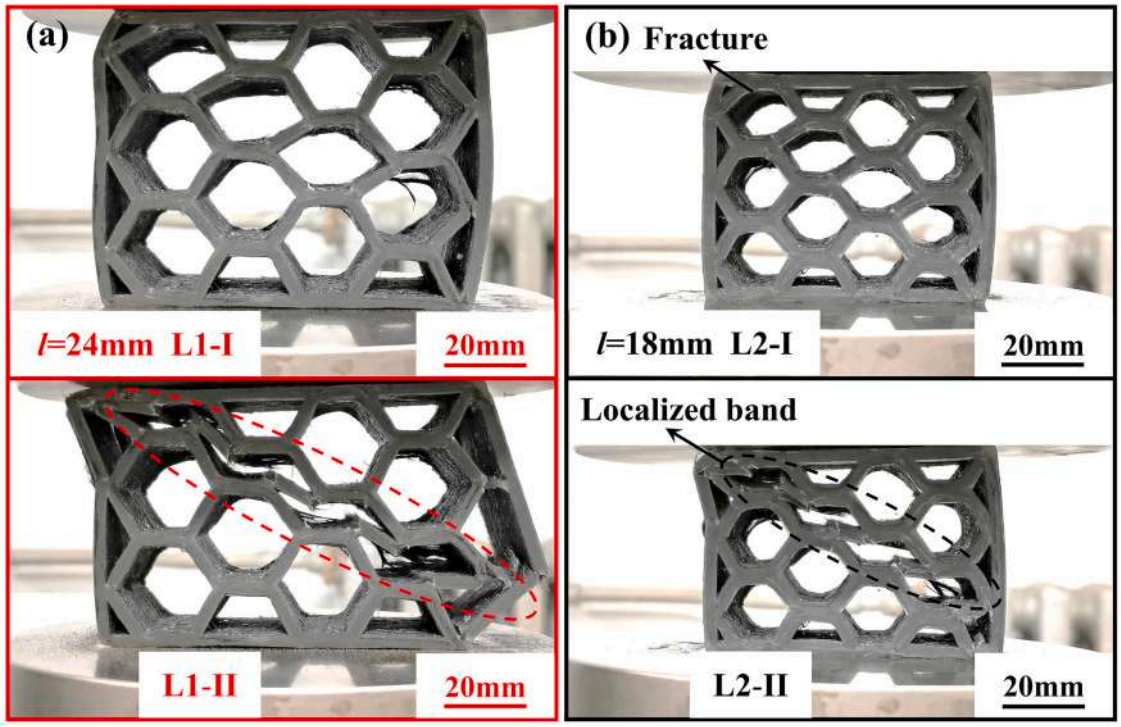

Fig. 12. In-plane compression failure modes of the 3D printed CFRCHSs with (a) $l = 24$ mm, $\varphi = 63^\circ$ and (b) $l = 18$ mm, $\varphi = 63^\circ$.

where E_s is the compression modulus of the parent material. Based on the basic beam theory, the following balance equations can be obtained from the symmetric boundary condition:

$$\frac{F_S\lambda^2}{2E_sI} - \frac{M_0\lambda}{E_sI} = 0 \tag{7}$$

$$\frac{F_S\lambda^3}{3E_sI} - \frac{M_0\lambda^2}{2E_sI} = \delta_S \tag{8}$$

From Eqs. (7) and (8), the shear force F_S of the supporting member is

$$F_S = \frac{12E_sI}{\lambda^3}\delta\cos\varphi \tag{9}$$

where, $I = bt^3/12$. From Eqs. (6) and (9), the total force F in the z-direction is as follows

$$F = F_N\sin\varphi + F_S\cos\varphi = \frac{E_sbt\delta}{\lambda}\left(\sin^2\varphi + \frac{t^2}{\lambda^2}\cos^2\varphi\right) \tag{10}$$

Then, the equivalent stress σ_F and strain ε_F applied to the honeycomb cell are obtained by the following equations:

$$\sigma_F = \frac{F}{b(\lambda\cos\varphi + l)} = \frac{E_st\delta}{\lambda(\lambda\cos\varphi + l)}\left(\sin^2\varphi + \frac{t^2}{\lambda^2}\cos^2\varphi\right) \tag{11}$$

$$\varepsilon_F = \frac{\delta}{\lambda\sin\varphi} \tag{12}$$

Combining Eqs. (11) and (12), the effective compression modulus E_c of the honeycomb cell is

$$E_c = \frac{t\sin\varphi E_s}{(\lambda\cos\varphi + l)}\left(\sin^2\varphi + \frac{t^2}{\lambda^2}\cos^2\varphi\right) \tag{13}$$

The equivalent in-plane compression modulus of CFRCHSs with two side panels is:

$$\overline{E} = E_s\frac{2t}{L} + E_c\frac{L-2t}{L} \tag{14}$$

where L is the length of CFRCHSs. During the in-plane compression process, the panels on both sides of CFRCHSs fail first. Therefore, the compression strength σ_{pk} of CFRCHSs holds the following relationship with the compression strength σ_c of the parent material:

$$\frac{\sigma_c}{E_s} = \frac{\sigma_{pk}}{\overline{E}} \tag{15}$$

From Eqs. (14) and (15), the in-plane compression strength of CFRCHSs is given as

$$\sigma_{pk} = \frac{\overline{E}}{E_s}\sigma_c = \left(\frac{2t}{L} + \frac{E_c}{E_s}\frac{L-2t}{L}\right)\sigma_c \tag{16}$$

The initial peak stress predictions of the 3D printed CFRCHSs with different honeycomb parameters under in-plane compression are obtained by applying Eq. (16). Fig. 19 summarizes the measured results of the honeycomb structures corresponding to the determined honeycomb parameters and compares the measurements with the analytical predictions. Since the FFF 3D printing process may cause defects in the honeycomb web and voids at the bonding interface, the measured initial peak stress of CFRCHSs is somewhat lower than the theoretical strength. Nevertheless, there is generally a good agreement between experimental measurements and analytical predictions. It can be found through careful observation that when the element lengths are the same, the honeycomb structure corresponding to $\varphi = 52^\circ$ exhibits the lowest compression strength, which indicates that a too-small inclination angle is undesirable in practical applications. To validate the analysis model more conveniently, the corresponding initial peak stress predictions are added to Figs. 11 and 14. The predictions close to but slightly greater than the initial peak stress of the equivalent stress-strain curves are observed.

3.3. Shape memory properties

Fig. 20 presents the detailed thermally induced shape recovery process of the 3D printed CFRCHSs. At an ambient temperature of 70 °C (above Tg), the shape memory PLA matrix in the rubbery state exhibits

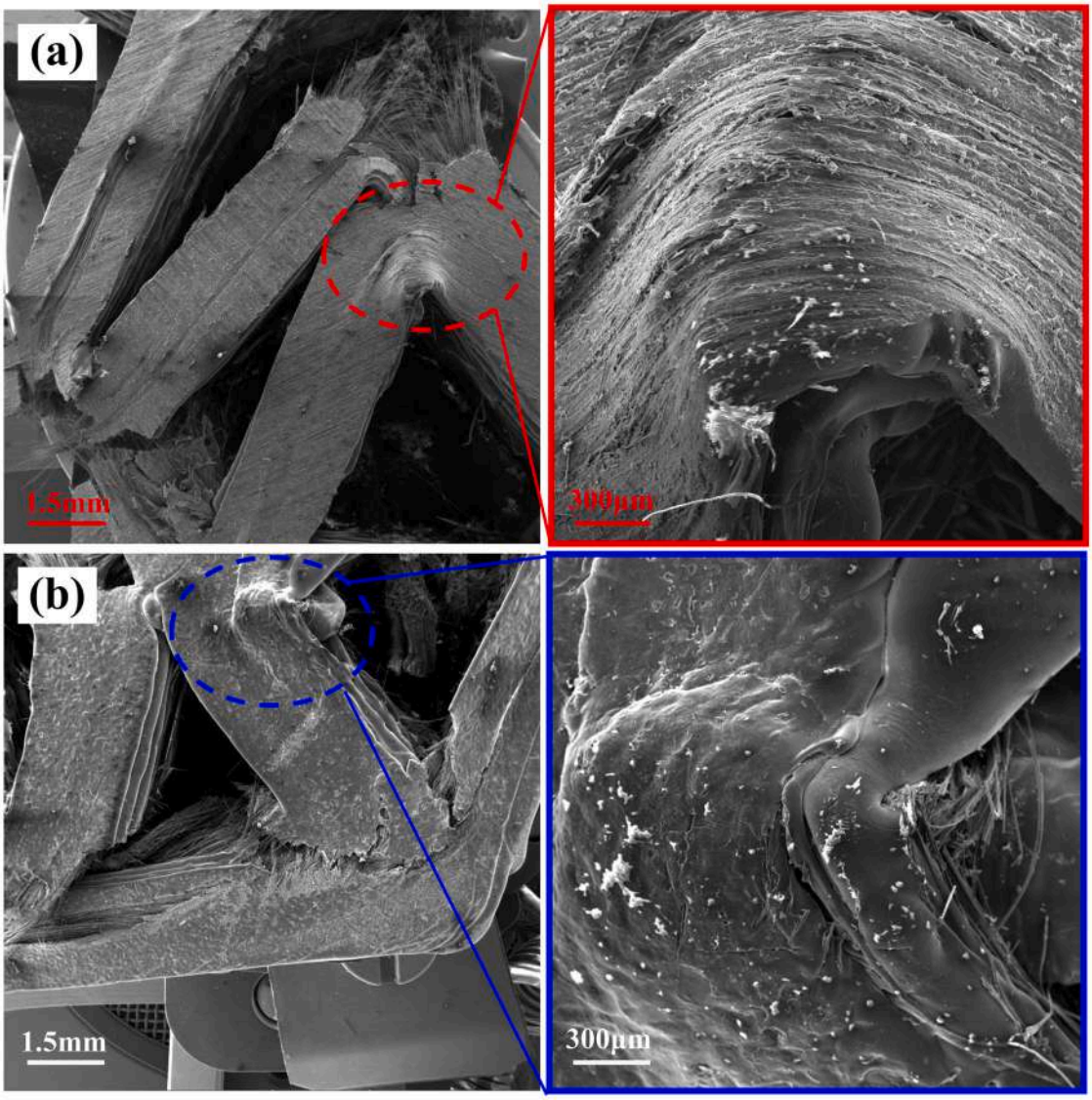

Fig. 13. SEM images of the failure surfaces of the 3D printed CFRCHSs after in-plane compression testing. (a) $l = 24$ mm, $\varphi = 63°$. (b) $l = 18$ mm, $\varphi = 63°$.

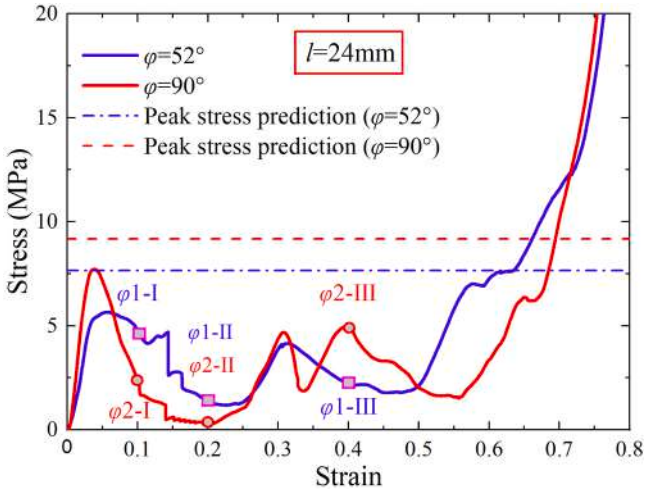

Fig. 14. The equivalent stress-strain curves of the 3D printed CFRCHSs with various inclination angles under in-plane compression.

great deformability and low elastic modulus. Therefore, compared with room temperature conditions, the 3D printed CFRCHSs possess lower stiffness and greater deformability at 70 °C. It is easy to implement compression and shaping at this temperature and the structure is not easy to be damaged. Comparing the deformed shape in Fig. 20b with the original shape in Fig. 20a, it can be seen that although the amount of deformation during the shaping process is as high as 50%, the honeycomb structure has not suffered an observable fracture.

Fig. 20b–e present the shape recovery process of the 3D printed CFRCHSs, which is completed within 20 s. In order to evaluate the shape recovery capacity, here the shape recovery ratio is defined as Shape recovery ratio $= (H_T - H_{def})/(H_{ori} - H_{def}) \times 100\%$, where H_{def} and H_T are respectively the height of the sample after being shaped and the height of the sample in the recovery process at the time T. Fig. 20f plots the evolution curve of the shape recovery ratio of the 3D printed CFRCHSs with heating time T. The shape recovery ratio remains unchanged within the first 6 s, because it takes a while to fully heat the sample. After that, the sample starts to recover quickly, which is associated with rapid glass transition and strain energy release. It can be found that the maximum shape recovery ratio of the 3D printed CFRCHSs is about 95%, which proves their excellent shape memory performance. Due to the shape memory effects, the 3D printed CFRCHSs hold more potential

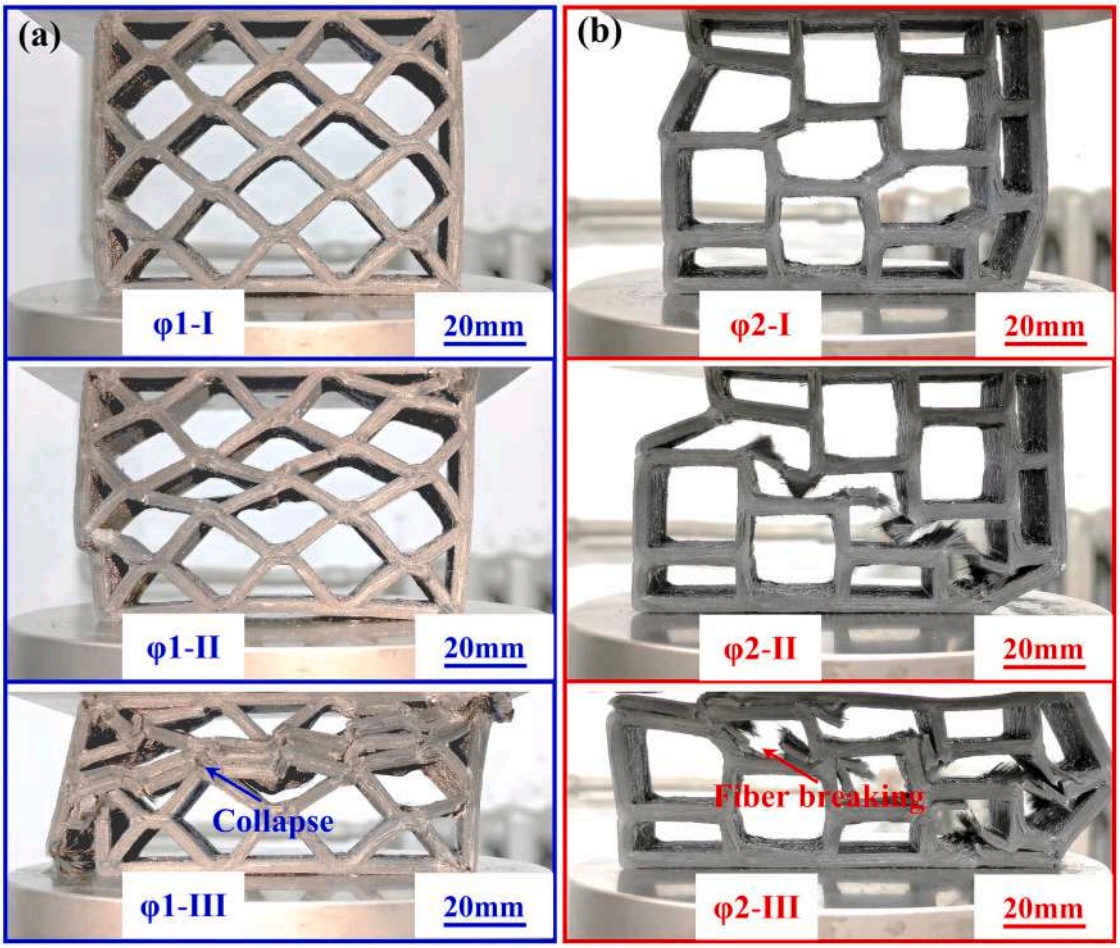

Fig. 15. In-plane compression failure modes of the 3D printed CFRCHSs with (a) $l = 24$ mm, $\varphi = 52°$ and (b) $l = 24$ mm, $\varphi = 90°$.

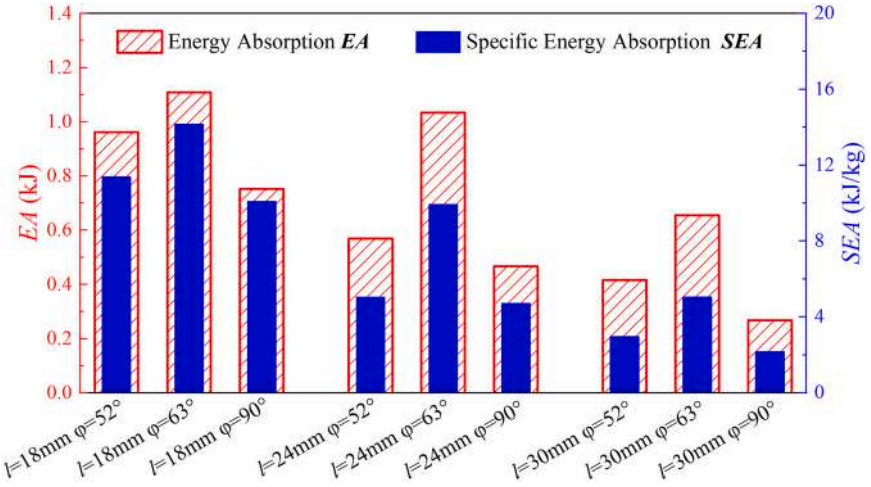

Fig. 16. Comparison of *EA* and *SEA* of the 3D printed CFRCHSs under the in-plane compression tests.

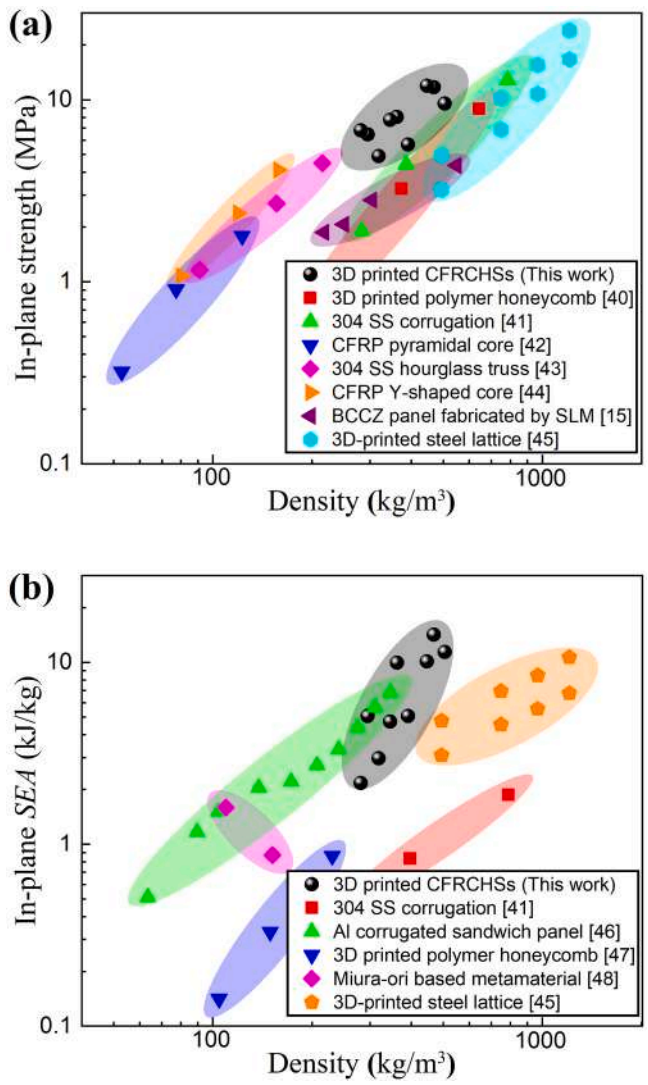

Fig. 17. Comparison of (a) compression strength and (b) *SEA* between the 3D printed CFRCHSs and competitive cellular topologies under in-plane compression.

applications than general metal or composite honeycomb structures. For instance, based on the concept of an active honeycomb structure for morphing wingtip applications proposed by Sun et al. [49], applying the 3D printed CFRCHSs for lightweight morphing wing can achieve thermally driven deformation of the wing.

4. Conclusions

CFRCHSs with shape memory effects were manufactured through an FFF-based 3D printing process. The experimental results indicate that the failure modes of the 3D printed CFRCHSs under out-of-plane loading are mainly lateral shearing and progressive folding failure. The excellent out-of-plane specific energy absorption of CFRCHSs is observed than several competitive cellular structures [1,9,34,36–39]. The in-plane crushing process of the 3D printed CFRCHSs is accompanied by the formation of the lateralized localized bands, which causes fluctuations in stress evolution. The crashworthiness analysis indicates that the 3D printed CFRCHSs outperform some competitive cellular topologies in terms of in-plane specific energy absorption [41,45–48]. Besides, a simplified analytical model for the initial in-plane compression strength of CFRCHSs was derived, and good agreement between experimental measurements and analytical predictions was observed. Thermally-induced shape recovery tests show that the 3D printed CFRCHSs have a maximum shape recovery ratio of 95% when the in-plane compression strain is as high as 50%, which demonstrates their great potential in lightweight intelligent structures.

These findings highlight the role of honeycomb parameters in improving the compression behavior and energy absorption capacity of the 3D printed CFRCHSs, and provide guidance for applying 3D printed CFRCHSs to multi-functional applications including lightweight intelligent systems and energy absorbing devices.

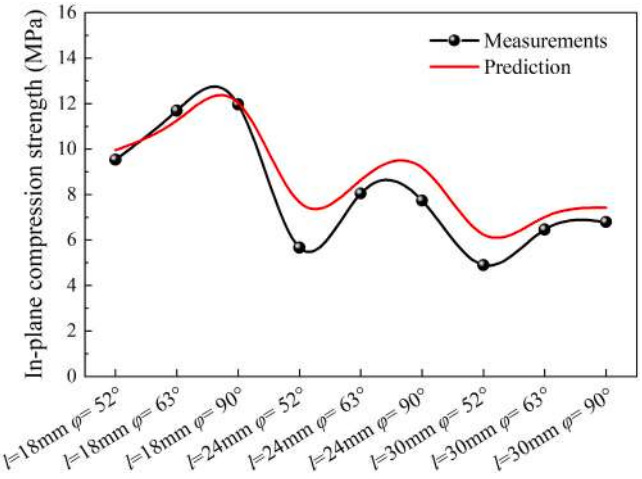

Fig. 19. Comparison of the predicted results of the in-plane compression strength of the 3D printed CFRCHSs with the experimental ones.

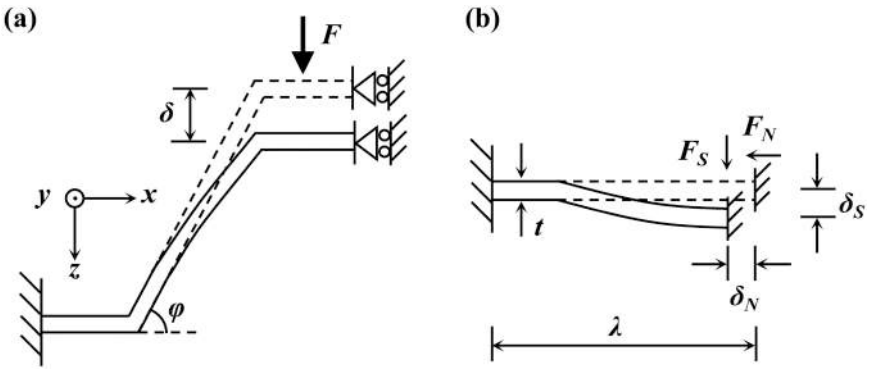

Fig. 18. Schematic diagram of honeycomb cell under in-plane compression loading. (a) A quarter cell and (b) the inclined web. Dotted and solid lines denote separately the initial and deformed web.

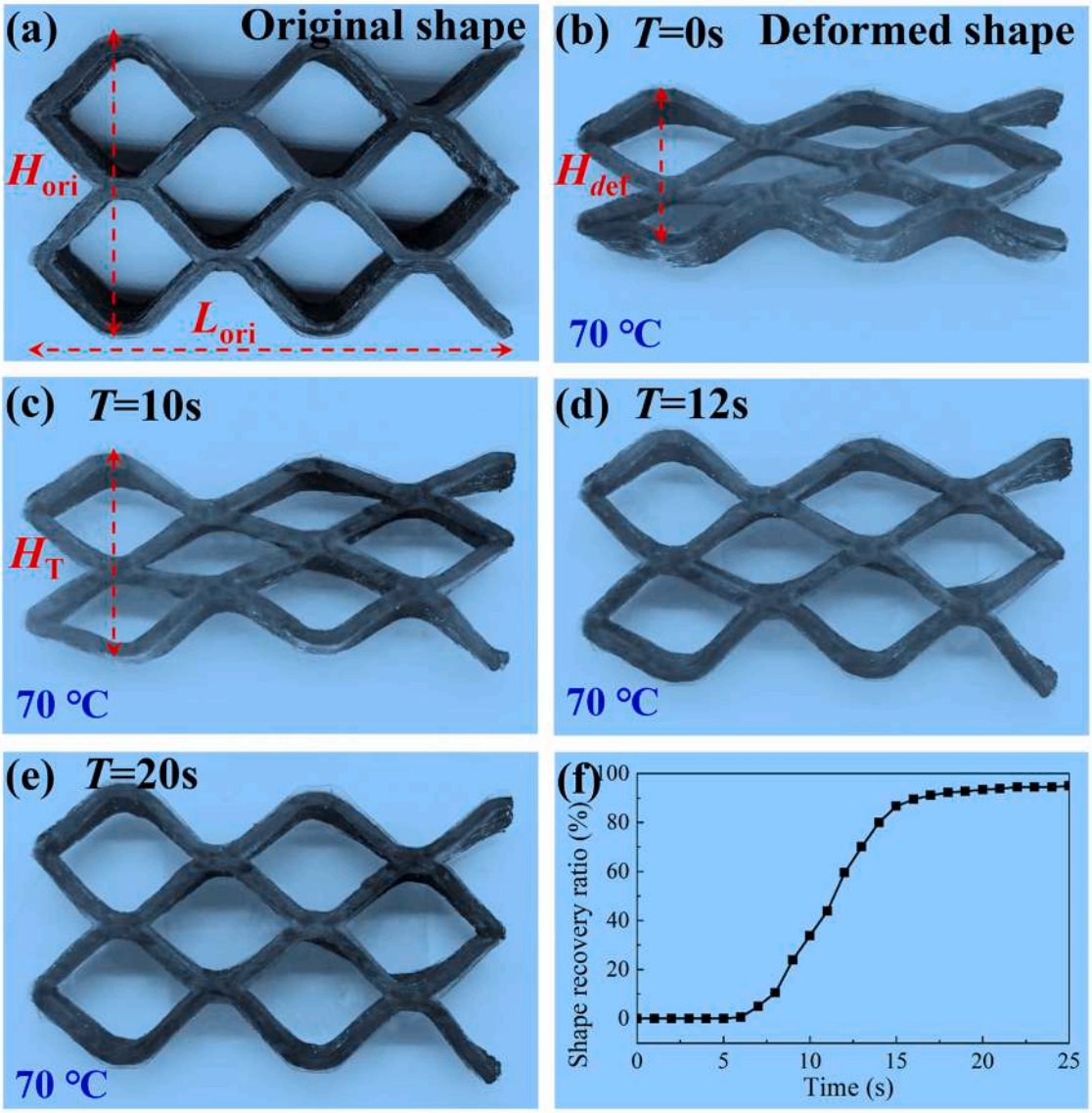

Fig. 20. Thermally-induced shape recovery behavior of the 3D printed CFRCHS. (a) The sample before being shaped. (b-e) The shape recovery process of the sample. (f) Shape recovery ratio versus time curve of the sample.

CRediT authorship contribution statement

Chengjun Zeng: Conceptualization, Investigation, Visualization, Formal analysis, Writing - original draft, Writing - review & editing. **Liwu Liu**: Methodology, Data curation, Validation, Writing - review & editing. **Wenfeng Bian**: Visualization, Data Curation, Writing - review & editing. **Jinsong Leng**: Conceptualization, Investigation, Writing - review & editing. **Yanju Liu**: Investigation, Writing - review & editing, Supervision.

Declaration of Competing Interest

The authors declare that they have no known competing financial interests or personal relationships that could have appeared to influence the work reported in this paper.

Acknowledgements

This work is supported by the National Natural Science Foundation of China (Grant Nos. 11632005, 11672086).

References

[1] X. Wei, D. Li, J. Xiong, Fabrication and mechanical behaviors of an all-composite sandwich structure with a hexagon honeycomb core based on the tailor-folding approach, Compos. Sci. Technol. 184 (2019), 107878, https://doi.org/10.1016/j.compscitech.2019.107878.
[2] Z. Zhang, H. Lei, M. Xu, J. Hua, C. Li, D. Fang, Out-of-plane compressive performance and energy absorption of multi-layer graded sinusoidal corrugated sandwich panels, Mater. Des. 178 (2019), 107858, https://doi.org/10.1016/j.matdes.2019.107858.
[3] V.H. Carneiro, S.D. Rawson, H. Puga, J. Meireles, P.J. Withers, Additive manufacturing assisted investment casting: a low-cost method to fabricate periodic metallic cellular lattices, Addit. Manuf. 33 (2020), 101085, https://doi.org/10.1016/j.addma.2020.101085.
[4] M. Kucewicz, P. Baranowski, J. Małachowski, A. Popławski, P. Płatek, Modelling, and characterization of 3D printed cellular structures, Mater. Des. 142 (2018) 177–189, https://doi.org/10.1016/j.matdes.2018.01.028.
[5] S. Hou, C. Shu, S. Zhao, T. Liu, X. Han, Q. Li, Experimental and numerical studies on multi-layered corrugated sandwich panels under crushing loading, Compos. Struct. 126 (2015) 371–385, https://doi.org/10.1016/j.compstruct.2015.02.039.
[6] L.J. Feng, Z.T. Yang, G.C. Yu, X.J. Chen, L.Z. Wu, Compressive and shear properties of carbon fiber composite square honeycombs with optimized high-modulus hierarchical phases, Compos. Struct. 201 (2018) 845–856, https://doi.org/10.1016/j.compstruct.2018.06.080.
[7] J. Souza, A. Großmann, C. Mittelstedt, Micromechanical analysis of the effective properties of lattice structures in additive manufacturing, Addit. Manuf. 23 (2018) 53–69, https://doi.org/10.1016/j.addma.2018.07.007.

[8] X. Xin, L. Liu, Y. Liu, J. Leng, Origami-inspired self-deployment 4D printed honeycomb sandwich structure with large shape transformation, Smart Mater. Struct. 29 (6) (2020), 065015, https://doi.org/10.1088/1361-665X/ab85a4.

[9] H.B. Rebelo, D. Lecompte, C. Cismasiu, A. Jonet, B. Belkassem, A. Maazoun, Experimental and numerical investigation on 3D printed PLA sacrificial honeycomb cladding, Int. J. Impact Eng. 131 (2019) 162–173, https://doi.org/10.1016/j.ijimpeng.2019.05.013.

[10] A. Kumar, L. Collini, A. Daurel, J.-Y. Jeng, Design and additive manufacturing of closed cells from supportless lattice structure, Addit. Manuf. 33 (2020), 101168, https://doi.org/10.1016/j.addma.2020.101168.

[11] L. Azzouz, Y. Chen, M. Zarrelli, J.M. Pearce, L. Mitchell, G. Ren, M. Grasso, Mechanical properties of 3-D printed truss-like lattice biopolymer non-stochastic structures for sandwich panels with natural fibre composite skins, Compos. Struct. 213 (2019) 220–230, https://doi.org/10.1016/j.compstruct.2019.01.103.

[12] L. Zhang, S. Feih, S. Daynes, S. Chang, M.Y. Wang, J. Wei, W.F. Lu, Energy absorption characteristics of metallic triply periodic minimal surface sheet structures under compressive loading, Addit. Manuf. 23 (2018) 505–515, https://doi.org/10.1016/j.addma.2018.08.007.

[13] D.S.J. Al-Saedi, S.H. Masood, M. Faizan-Ur-Rab, A. Alomarah, P. Ponnusamy, Mechanical properties and energy absorption capability of functionally graded F2BCC lattice fabricated by SLM, Mater. Des. 144 (2018) 32–44, https://doi.org/10.1016/j.matdes.2018.01.059.

[14] P. Baranowski, P. Płatek, A. Antolak-Dudka, M. Sarzyński, M. Kucewicz, T. Durejko, J. Małachowski, J. Janiszewski, T. Czujko, Deformation of honeycomb cellular structures manufactured with Laser Engineered Net Shaping (LENS) technology under quasi-static loading: experimental testing and simulation, Addit. Manuf. 25 (2019) 307–316, https://doi.org/10.1016/j.addma.2018.11.018.

[15] C. Li, H. Lei, Y. Liu, X. Zhang, J. Xiong, H. Zhou, D. Fang, Crushing behavior of multi-layer metal lattice panel fabricated by selective laser melting, Int. J. Mech. Sci. 145 (2018) 389–399, https://doi.org/10.1016/j.ijmecsci.2018.07.029.

[16] S. Kumar, J. Ubaid, R. Abishera, A. Schiffer, V.S. Deshpande, Tunable energy absorption characteristics of architected honeycombs enabled via additive manufacturing, ACS Appl. Mater. Inter. 11 (45) (2019) 42549–42560, https://doi.org/10.1021/acsami.9b12880.

[17] D.J. McGregor, S. Tawfick, W.P. King, Mechanical properties of hexagonal lattice structures fabricated using continuous liquid interface production additive manufacturing, Addit. Manuf. 25 (2019) 10–18, https://doi.org/10.1016/j.addma.2018.11.002.

[18] F. Li, L. Liu, X. Lan, X. Zhou, W. Bian, Y. Liu, J. Leng, Preliminary design and analysis of a cubic deployable support structure based on shape memory polymer composite, Int. J. Smart Nano Mater. 7 (2016) 106–118, https://doi.org/10.1080/19475411.2016.1212948.

[19] W. Zhang, F. Zhang, X. Lan, J. Leng, A.S. Wu, T.M. Bryson, C. Cotton, B. Gu, B. Sun, T.-W. Chou, Shape memory behavior and recovery force of 4D printed textile functional composites, Compos. Sci. Technol. 160 (2018) 224–230, https://doi.org/10.1016/j.compscitech.2018.03.037.

[20] R. Tao, L. Xi, W. Wu, Y. Li, B. Liao, L. Liu, J. Leng, D. Fang, 4D printed multi-stable metamaterials with mechanically tunable performance, Compos. Struct. 252 (2020), 112663, https://doi.org/10.1016/j.compstruct.2020.112663.

[21] C. Yang, M. Boorugu, A. Dopp, J. Ren, R. Martin, D. Han, W. Choi, H. Lee, 4D printing reconfigurable, deployable and mechanically tunable metamaterials, Mater. Horiz. 6 (6) (2019) 1244–1250, https://doi.org/10.1039/c9mh00302a.

[22] R.D. Hussein, D. Ruan, G. Lu, I. Sbarski, Axial crushing behaviour of honeycomb-filled square carbon fibre reinforced plastic (CFRP) tubes, Compos. Struct. 140 (2016) 166–179, https://doi.org/10.1016/j.compstruct.2015.12.064.

[23] J.M. Chacón, M.A. Caminero, P.J. Núñez, E. García-Plaza, I. García-Moreno, J. M. Reverte, Additive manufacturing of continuous fibre reinforced thermoplastic composites using fused deposition modelling: Effect of process parameters on mechanical properties, Compos. Sci. Technol. 181 (2019), 107688, https://doi.org/10.1016/j.compscitech.2019.107688.

[24] M.A. Caminero, J.M. Chacón, I. García-Moreno, G.P. Rodríguez, Impact damage resistance of 3D printed continuous fibre reinforced thermoplastic composites using fused deposition modelling, Compos. Part B Eng. 148 (2018) 93–103, https://doi.org/10.1016/j.compositesb.2018.04.054.

[25] Z. Hou, X. Tian, J. Zhang, D. Li, 3D printed continuous fibre reinforced composite corrugated structure, Compos. Struct. 184 (2018) 1005–1010, https://doi.org/10.1016/j.compstruct.2017.10.080.

[26] Y. Ming, S. Zhang, W. Han, B. Wang, Y. Duan, H. Xiao, Investigation on process parameters of 3D printed continuous carbon fiber-reinforced thermosetting epoxy composites, Addit. Manuf. 33 (2020), 101184, https://doi.org/10.1016/j.addma.2020.101184.

[27] C. Quan, B. Han, Z. Hou, Q. Zhang, X. Tian, T.-J. Lu, 3D printed continuous fiber reinforced composite auxetic honeycomb structures, Compos. Part B Eng. 187 (2020), 107858, https://doi.org/10.1016/j.compositesb.2020.107858.

[28] K. Essassi, J.L. Rebiere, A. El Mahi, M.A. Ben Souf, A. Bouguecha, M. Haddar, Experimental and analytical investigation of the bending behaviour of 3D-printed bio-based sandwich structures composites with auxetic core under cyclic fatigue tests, Compos. Part A Appl. Sci. Manuf. 131 (2020), 105775, https://doi.org/10.1016/j.compositesa.2020.105775.

[29] K. Sugiyama, R. Matsuzaki, M. Ueda, A. Todoroki, Y. Hirano, 3D printing of composite sandwich structures using continuous carbon fiber and fiber tension, Compos. Part A Appl. Sci. Manuf. 113 (2018) 114–121, https://doi.org/10.1016/j.compositesa.2018.07.029.

[30] S. Liu, Y. Li, N. Li, A novel free-hanging 3D printing method for continuous carbon fiber reinforced thermoplastic lattice truss core structures, Mater. Des. 137 (2018) 235–244, https://doi.org/10.1016/j.matdes.2017.10.007.

[31] Z. Wang, C. Luan, G. Liao, X. Yao, J. Fu, Mechanical and self-monitoring behaviors of 3D printing smart continuous carbon fiber-thermoplastic lattice truss sandwich structure, Compos. Part B Eng. 176 (2019), 107215, https://doi.org/10.1016/j.compositesb.2019.107215.

[32] C. Zeng, L. Liu, W. Bian, Y. Liu, J. Leng, 4D printed electro-induced continuous carbon fiber reinforced shape memory polymer composites with excellent bending resistance, Compos. Part B Eng. 194 (2020), 108034, https://doi.org/10.1016/j.compositesb.2020.108034.

[33] Y. Du, C. Song, J. Xiong, L. Wu, Fabrication and mechanical behaviors of carbon fiber reinforced composite foldcore based on curved-crease origami, Compos. Sci. Technol. 174 (2019) 94–105, https://doi.org/10.1016/j.compscitech.2019.02.019.

[34] G. Sun, S. Li, Q. Liu, G. Li, Q. Li, Experimental study on crashworthiness of empty/aluminum foam/honeycomb-filled CFRP tubes, Compos. Struct. 152 (2016) 969–993, https://doi.org/10.1016/j.compstruct.2016.06.019.

[35] S.J.A. Kumar, K.S. Ahmed, Compression behavior and energy absorption capacity of stiffened syntactic foam core sandwich composites, J. Reinf. Plast. Compos. 32 (18) (2013) 1370–1379, https://doi.org/10.1177/0731684413492867.

[36] F. Côté, V.S. Deshpande, N.A. Fleck, A.G. Evans, The out-of-plane compressive behavior of metallic honeycombs, Mater. Sci. Eng. A 380 (1–2) (2004) 272–280, https://doi.org/10.1016/j.msea.2004.03.051.

[37] H. Liu, L. Chen, B. Du, S. Peng, Y. Guo, Y. Zhao, L. Chen, H. Zhou, W. Li, P. Liu, Flatwise compression property of hierarchical thermoplastic composite square lattice, Compos. Struct. 210 (2019) 118–133, https://doi.org/10.1016/j.compstruct.2018.11.047.

[38] Z. Wang, Z. Lu, H. Tian, S. Yao, W. Zhou, Theoretical assessment methodology on axial compressed hexagonal honeycomb's energy absorption capability, Mech. Adv. Mater. Struct. 23 (5) (2015) 503–512, https://doi.org/10.1080/15376494.2014.994150.

[39] Y. Zhang, T. Chen, X. Xu, Z. Hu, Out-of-plane mechanical behaviors of a side hierarchical honeycomb, Mech. Mater. 140 (2020), 103227, https://doi.org/10.1016/j.mechmat.2019.103227.

[40] Y. Chen, T. Li, Z. Jia, F. Scarpa, C.-W. Yao, L. Wang, 3D printed hierarchical honeycombs with shape integrity under large compressive deformations, Mater. Des. 137 (2018) 226–234, https://doi.org/10.1016/j.matdes.2017.10.028.

[41] B. Han, L. Yan, B. Yu, Q. Zhang, C. Chen, T.-J. Lu, Collapse mechanisms of metallic sandwich structures with aluminum foam-filled corrugated cores, J. Mech. Mater. Struct. 9 (2014) 397–425, https://doi.org/10.2140/jomms.2014.9.397.

[42] J. Xiong, L. Ma, A. Vaziri, J. Yang, L. Wu, Mechanical behavior of carbon fiber composite lattice core sandwich panels fabricated by laser cutting, Acta Mater. 60 (2012) 5322–5334, https://doi.org/10.1016/j.actamat.2012.06.004.

[43] L.J. Feng, L.Z. Wu, G.C. Yu, An Hourglass truss lattice structure and its mechanical performances, Mater. Des. 99 (2016) 581–591, https://doi.org/10.1016/j.matdes.2016.03.100.

[44] J. Liu, J. Liu, J. Mei, W. Huang, Investigation on manufacturing and mechanical behavior of all-composite sandwich structure with Y-shaped cores, Compos. Sci. Technol. 159 (2018) 87–102, https://doi.org/10.1016/j.compscitech.2018.01.026.

[45] X. Cao, S. Duan, J. Liang, W. Wen, D. Fang, Mechanical properties of an improved 3D-printed rhombic dodecahedron stainless steel lattice structure of variable cross section, Int. J. Mech. Sci. 145 (2018) 53–63, https://doi.org/10.1016/j.ijmecsci.2018.07.006.

[46] C. Shu, S. Zhao, S. Hou, Crashworthiness analysis of two-layered corrugated sandwich panels under crushing loading, Thin Walled Struct. 133 (2018) 42–51, https://doi.org/10.1016/j.tws.2018.09.008.

[47] F.N. Habib, P. Iovenitti, S.H. Masood, M. Nikzad, In-plane energy absorption evaluation of 3D printed polymeric honeycombs, Virtual Phys. Prototyp. 12 (2) (2017) 117–131, https://doi.org/10.1080/17452759.2017.1291354.

[48] J. Zhang, D. Karagiozova, Z. You, Y. Chen, G. Lu, Quasi-static large deformation compressive behaviour of origami-based metamaterials, Int. J. Mech. Sci. 153–154 (2019) 194–207, https://doi.org/10.1016/j.ijmecsci.2019.01.044.

[49] J. Sun, H. Gao, F. Scarpa, C. Lira, Y. Liu, J. Leng, Active inflatable auxetic honeycomb structural concept for morphing wingtips, Smart Mater. Struct. 23 (12) (2014), 125023, https://doi.org/10.1088/0964-1726/23/12/125023.